Pergamon

Phys. Chem. Earth (B), Vol. 25, No. 10–12, pp. 943–948, 2000
© 2000 Elsevier Science Ltd
All rights reserved
1464-1909/00/$ - see front matter

PII: S1464-1909(00)00130-1

Impact of Rainfall Incoherent Backscattering Upon Radar Echoes Above 10 GHz

F. S. Marzano[1], L. Roberti[2] and A. Mugnai[3]

[1]Dipartimento di Ingegneria Elettrica, Università dell'Aquila, Monteluco di Roio, 67040 L'Aquila, Italy
E-mail: marzano@ing.univaq.it
[2]Dipartimento di Elettronica, Politecnico di Torino, C.so Duca degli Abruzzi 24, 10129 Torino, Italy
E-mail: roberti@polito.it
[3]Istituto di Fisica dell'Atmosfera, Consiglio Nazionale delle Ricerche (CNR), Via Fosso del Cavaliere 99, 00123, Roma, Italy. E-mail: mugnai@ifa.rm.cnr.it

Received 14 June 2000; accepted 22 June 2000

Abstract. Radar observations of precipitation profiles from space are simulated in order to evaluate the impact of precipitation incoherent backscattering upon radar returns above 10 GHz at nadir. Spaceborne and airborne radar frequencies at 13.8, 24, and 35 GHz are chosen for carrying out simulations at nadir. Realistic precipitation profiles are extracted from a microphysical mesoscale cloud model simulation and averaged with respect to classes of surface rainrate. The classical radar equation is reformulated taking into account the multiple scattering phenomenon through a general definition of the *apparent* reflectivity. Numerical results show that opposite effects are due to the combination of path attenuation and multiple scattering. When first-order scattering approximation holds, path attenuation is the predominant contribution and tends to reduce the equivalent reflectivity, while multiple scattering tends to increase it, especially in the cloud regions characterized by large albedo. For intense rainfall cases the rainrate profiles can be significantly overestimated when derived from *apparent* radar reflectivity simply corrected by two-way single-scattering path attenuation.
© 2000 Elsevier Science Ltd. All rights reserved.

1. Introduction

Spaceborne and airborne radar sensing and profiling of precipitation has been well established in the last two decades (Meneghini, 1978; Fujita, 1983). Several rain retrieval techniques have been developed so far using both space-based radar reflectivity measurements and combined radiometric and radar data (Meneghini and Nakamura, 1990; Marzoug and Amayenc, 1994; Olson et al., 1996). The use of radar reflectivity measurements between 10 and 35 GHz has been investigated to estimate precipitation profiles from single-frequency, dual-frequency and dual-beam observations (Testud et al., 1992). The formulation of these estimation methods basically relies on the solution of the radar equation in an attenuating medium in either a deterministic or stochastic form (Iguchi and Meneghini, 1994; Haddad et al. 1996).

Correspondence to: F.S. Marzano

Further constraints, derived from either radiometric measurements or from surface-reference radar techniques, are generally added in the inverse problem in order to ensure the stability of the solution itself (Mongi and Amayenc, 1991; Marzano et al., 1999).

The radar equation in an attenuating medium, as generally stated, takes into account single scattering, due to raindrops, weighted by the path attenuation from the considered range gate to the radar antenna (Sauvageot, 1992). However, for frequencies higher than 10 GHz and for intense to heavy rainfall, the albedo of precipitating ice and liquid hydrometeors can be significant (Marzano et al., 1994). This means that multiple scattering effects can play a relevant role in determining the radar received power (Ito et al., 1995). Disregarding this multiply scattered radiation in the formulation of the radar forward problem could affect the accuracy of both the ranging and estimate of rainfall rate profile. Even though derived by using a simple rain-slab model, it has been shown that neglecting the multiple scattering effects due to intense rainfall can lead to an overestimation of rainrate higher than 50% (Oguchi et al., 1998).

The objective of this work is to evaluate the possible impact of the rainfall incoherent backscattering upon the radar response in the 10- to 40- GHz band through a numerical investigation based on cloud-model vertical profiles of precipitating liquid and ice hydrometeors. Spaceborne radar observations of precipitation profiles are simulated by means of a radiative transfer model, using a Monte Carlo solution technique. The effects of precipitation multiple scattering are evaluated at various attenuating frequencies and for nadir observations. The 13.8-GHz frequency band of frequency band of the Precipitation Radar (PR) aboard the Tropical Rainfall Measuring Mission (TRMM) is chosen together with the channels at 24 GHz and 35 GHz, already tested in airborne campaigns and explored for spaceborne applications (Meneghini and Nakamura, 1990; Kummerow et al. 1998). Sect. 2 illustrates how realistic precipitation profiles are extracted from the outputs of a three-dimensional microphysical mesoscale cloud model and characterized

through single-scattering optical parameters. The concept of radar *apparent* reflectivity is introduced in sect 3. Numerical results are shown and discussed in sect. 4 in terms of the observed *apparent* reflectivity, together with derived rainrate from 13.8-GHz data, for precipitation profiles going from low to intense precipitation.

2. Radar equation and single-scattering modeling

The meteorological radar equation in an attenuating medium relates the mean received power $<P_R(r)>$, obtained from the average of back-scattered pulses within a given range gate defining the scattering volume, to the transmitted power P_T, as follows (Sauvageot, 1992):

$$<P_R(r)> = C\, P_T\, Z_e(r)\, L^2(r) / r^2 \qquad (1)$$

where C is the radar instrumental constant, Z_e is the equivalent reflectivity factor of the range-gated scattering volume, $L(r)$ is the attenuation factor, and r is the distance between the radar antenna and the considered range gate. Only the scalar form of the radar equation is analyzed here, even though (1) might be easily extended to polarimetric measurements.

The one-way attenuation factor $L(r)$, indicating the total attenuation between the radar and the considered range gate, is given by:

$$L(r)= \exp[-\tau(r)]= \exp[-A(r)/4.343] = \exp[-\int_0^r k_e(r')\, dr'] \qquad (2)$$

where k_e is the range-dependent volumetric extinction coefficient and τ is the optical thickness such that the one-way path attenuation is $A(r)= 4.343\ \tau(r)$ (in dB). Even though in the radar literature τ generally indicates the pulse duration, here we have adopted the radiative transfer notation (Ishimaru, 1978; Tsang et al., 1985).

The radar instrumental constant C basically takes into account the antenna gain, the beamwidth, the pulse duration, the guidance losses, and the radar wavelength. Indeed, the constant C includes also a medium refractive-index term, which is usually assumed constant as it will be shown later. Other factors due to the implemented digital signal processing, as the matched filtering, can be also inserted in C. Notice that the range gate is generally supposed to be completely filled by the scattering volume, unless non-uniform beam filling corrections are considered.

In the following sections we will briefly introduce the mesoscale cloud model, where the precipitation profiles were extracted from, together with an overview of the single-scattering computations relevant to the radar equation in scattering media.

2.1 Extraction of synthetic precipitation profiles

The raining cloud profiles were obtained from the cloud microphysical-dynamical model developed by Tao et al. (1993). The cloud domain consists in 64 by 64 pixels, available every 15 minutes during the evolution of the simulated storm. A single time-step (minute 210 of GATE simulation), corresponding to the mature stage of a squall line over the Indian Ocean, was chosen in this study.

Each pixel consists of 28 vertical layers from the surface to a height of 18 km with a variable vertical resolution. The 28 layers of the original cloud model were re-sampled to 36 layers, each 0.5 km thickness. This choice was made in order to have the layer thickness compatible with a typical range resolution of a spaceborne radar.

For each grid cell the cloud model specifies height, pressure, temperature, relative humidity, together with cloud water, rain water, cloud ice, snow and graupel equivalent water contents (EWC's). Rain and graupel densities were set, respectively, to 1 g cm^{-3} and 0.4 g cm^{-3}. All hydrometeors' shape was assumed to be spherical. Even though the latter assumption is not strictly valid for large raindrops and ice crystals, this error was considered to be of second-order here. A Marshall-Palmer size distribution with a variable slope was used for snow, rain and graupel particles, while a modified Gamma was adopted for cloud droplets (Olson et al., 1996). The gaseous absorption was computed by the Liebe model.

In this work we have limited our analysis to plane-parallel atmospheric structures only so that some typical precipitation profiles were extracted from the cloud-model grid. In particular, 16 vertical columns (pixels) were selected in correspondence to 2 classes of surface rainrate around 5 and 50, each rainrate class having 8 pixels. The hydrometeor vertical profiles (and the associated meteorological variables) of each class were horizontally averaged. The result of this procedure was the generation of a set of 2 average profiles with a low (LRF) and intense (IRF) to be used for the numerical tests shown in sect. 4.

Fig. 1 shows the obtained average profiles of cloud (non-precipitating liquid), rain (precipitating liquid), graupel (precipitating ice), and snow (non-precipitating ice) equivalent water contents for the LRF and IRF cases. The intense rainfall profiles are characterized by a large amount of graupel and rain above and below the freezing level around 4.5 km, respectively, as typical for a convective updraft. The graupel vertical distribution, consistent with the rain one, is one of the major feature derived from mesoscale models, otherwise not usually included in *ad hoc* rain structures. Indeed, graupel amount in the GATE simulation seemed to be exaggerated in some convective cells (Olson et al., 1996). This is the reason why chose rainfall profiles not too intense from the simulation grid.

2.2 Simulation of single-scattering radar parameters

The volumetric equivalent (effective) reflectivity factor Z_e can be related to the backscattering properties of the precipitation volume by means of (Ishimaru, 1978):

$$Z_e = [\lambda^4 / (\pi^5 |K|^2)]\, \eta_e = [(\lambda^4 / (\pi^5 |K|^2)]\, p(\Omega_s=\pi)\, k_s \qquad (3)$$

where λ is the radar wavelength, K is the so-called dielectric factor (equal to 0.93 for water drops), η_e is the

volumetric equivalent radar reflectivity, $p(\Omega_s=\pi)$ is the volumetric scattering phase function computed in the backward direction (i.e., for the scattering solid angle Ω_s equal to π), and k_s is the volumetric scattering coefficient.

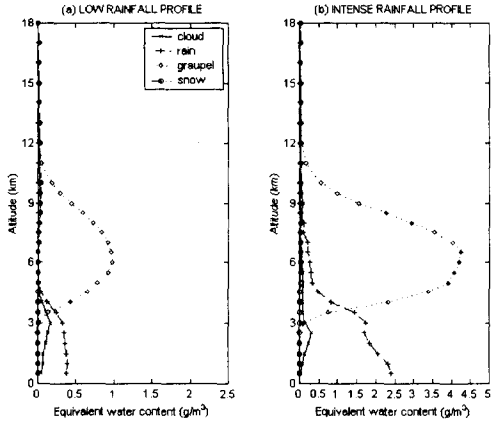

Fig. 1. Average vertical profiles of cloud, rain, graupel, and snow equivalent water contents (EWC's) for the low rainfall (LRF) and intense rainfall (IRF) cases.

Due to the sphericity assumption of the hydrometeors, the Mie theory was used for computing the single-scattering parameters. The Henyey-Greenstein approximation was assumed for the volumetric scattering phase function. Simulations were done at 3 different frequencies in the K and Ka band, that is at 13.8 (hereinafter, also referred to as 14 GHz), 24, and 35 GHz.

We can now illustrate the single-scattering (optical) parameters, as derived from the precipitation profiles shown in Fig. 1. In Fig. 2 the vertical profiles of the equivalent reflectivity factor Z_e is depicted at 14, 24, and 35 GHz for LRF and IRF as a function of the altitude h. Being all computations referred to nadir viewing, the radar range is actually along the altitude.

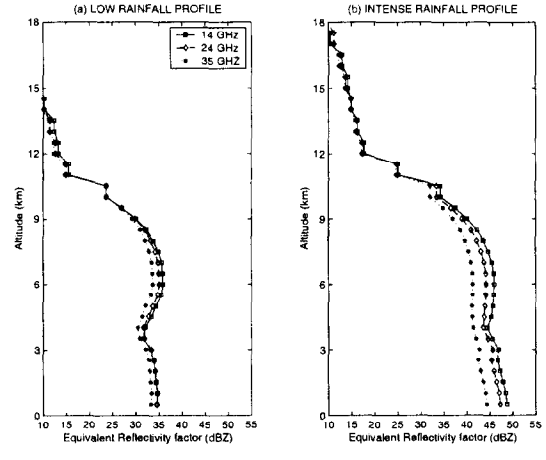

Fig. 2. Vertical profiles of equivalent reflectivity factor Z_e at 13.8 (or 14, for brevity), 24, and 35 GHz for the LRF and IRF cases, shown in Fig. 1, as a function of the altitude h (or radar range r with r=0 km at h=18 km).

High reflectivities (up to 50 dBZ) are obtained for the intense rainfall profile, especially in the rain layers below the freezing level around 4.5 km and in the graupel layers between 5 and 8 km, and for the lowest frequency at 14 GHz. As expected, Z decreases with the increase of frequency, that is with the decrease of wavelength (see (3)).

The one-way path attenuation A determines the attenuation factor L in (2). Values of total path attenuation (i.e., from the surface to the antenna) of about 10 dB are observed at 14 GHz for the IRF case, while at 35 GHz values of total A can reach about 10 dB in the LRF case (not shown). The impact of path attenuation will reflect on the observed (attenuated) reflectivities.

As already said, the albedo w above 10 GHz can be significant for high rainrates. This should be an indicator of the importance of the multiple scattering effects, since the albedo weights the multiple scattering term in the radiative transfer (Tsang et al., 1985). Numerical simulations (not shown) suggest that at 14 GHz w is generally less than 0.8, even around heights of 4-8 km where the graupel scattering plays the major role at all frequencies. At 35 GHz w can be as high as 0.95 around the graupel concentration peaks.

3. Incoherent backscattering and *apparent* reflectivity

The classical radar equation is derived under the assumption of single-scattering conditions and can include path attenuation, as shown by (1). However, in general conditions of multiple scattering, we expect the mean received power $\langle P_R(r)\rangle_{MS}$ to be different (higher) with respect to $\langle P_R(r)\rangle$. If $\langle I_R(r)\rangle_{MS}$ [W m^{-2} sr^{-1} Hz^{-1}] is the received mean specific intensity due to the range gate at distance r, then the multiply scattered received power $\langle P_R(r)\rangle_{MS}$ can be expressed as (Ishimaru, 1978):

$$\langle P_R(r)\rangle_{MS} = \int_{4\pi} A_e(\Omega') \langle I_R(\Omega',r)\rangle_{MS} \, d\Omega' \qquad (4)$$

with $A_e(\Omega)=A_{eo}|f_n(\Omega)|^2$, being $A_{eo}=A_e(\Omega_o)$ the maximum antenna equivalent area (in the Ω_o direction) and $|f_n(\Omega)|^2$ the normalized radiation pattern.

For a narrow-beam antenna, $\langle I_R(\Omega,r)\rangle_{MS}$ can be assumed constant within the antenna main lobe so that (4) reduces to:

$$\langle P_R(r)\rangle_{MS} \cong A_{eo}\, \Omega_A \langle I_R(\Omega_o,r)\rangle_{MS} \qquad (5a)$$

where Ω_o is the pointing angle of the radar antenna and Ω_A is the main-lobe solid angle, given by:

$$\Omega_A = \int_{\Omega_M} |f_n(\Omega')|^2 \, d\Omega' \qquad (5b)$$

with Ω_M the main-lobe angular width. Notice that the narrow-beam approximation is introduced for simplicity and it does not flaw the generality of our conclusions.

In the far-field zone the transmitted power P_T can be related to the power flux density F_T [W m^{-2} Hz^{-1}] through:

$$F_T(\Omega,r) = P_T G(\Omega) / (4\pi r^2) \quad (6)$$

where $G(\Omega)$ is the antenna gain such that $G(\Omega)=G_o |f_n(\Omega')|^2$ with $G_o=G(\Omega_o)$ the maximum gain. The latter is related to the maximum antenna equivalent area A_{eo} through the reciprocity formula, that is $G_o=4\pi(A_{eo}/\lambda^2)$.

Let us define in a multiple scattering medium the volumetric *apparent* radar reflectivity η_{aMS} at a range r and in the direction Ω in a way analogous to the surface scattering coefficient σ^0 (Tsang et al., 1985), that is:

$$\eta_{aMS}(\Omega,r) \equiv (4\pi/\Delta r) [<I_R(\Omega,r)>_{MS} / F_T(\Omega,r)] \quad (7)$$

being $\Delta r=c\Delta t/2$ the range resolution with Δt the pulse width and c the light velocity. Equation (7) basically expresses the *apparent* reflectivity as a radar scattering cross-section per unit volume.

Using (7), it is straightforward in the narrow-beam approximation to re-express (5) in terms of the *apparent* reflectivity η_{aMS} as follows:

$$<P_R(r)>_{MS} \equiv [G_o A_{eo} \Omega_A \Delta r / (4\pi)^2] (P_T / r^2) \eta_{aMS}(\Omega_o,r) \quad (8)$$

But, in analogy to (3), the *apparent* radar reflectivity can be expressed in the Ω_o direction through the *apparent* reflectivity factor Z_{aMS}:

$$Z_{aMS}(\Omega_o,r) = [\lambda^4 / (\pi^5 |K|^2)] \eta_{aMS}(\Omega_o,r) \quad (9)$$

By substituting (9) in (8), we can obtained an equation which resembles the radar equation given in (1), that is:

$$<P_R(r)>_{MS} \equiv C P_T Z_{aMS}(\Omega_o,r) / r^2 \quad (10)$$

where the radar constant C is given by:

$$C = [(A_{eo}G_o \Omega_A \Delta r) / (4\pi)^2] / [\lambda^4 / (\pi^5 |K|^2)] \quad (11)$$

Expression (11) basically justifies the comments about the radar instrumental constant C, first introduced in (1). Note that in (11) the receiver losses were neglected and the term Ω_A is basically the narrow-beam approximation of the beamwidth factor, expressed as the angular integral of $|f_n(\Omega)|^4$ (Sauvageot, 1992). Equation (10) is also valid under the assumption of a uniform distribution of the random scatterers within the main beam (i.e., neglecting the non-uniform beam filling of the range volume).

The generalized radar equation (10) can be simplified when considering only first-order scattering phenomena by introducing the first-order scattering *apparent* reflectivity factor Z_{aFS}. As a special case of (7), we can define Z_{aFS} as:

$$Z_{aFS}(\Omega_o,r)=[\lambda^4/(\pi^5|K|^2)][4\pi<I_R(\Omega_o,r)>_{FS}]/[F_T(\Omega_o,r)\Delta r] \quad (12a)$$

where $<I_R(\Omega_o,r)>_{FS}$ is the received specific intensity in the first-order scattering approximation. From the radiative transfer theory, it can be demonstrated that (Ishimaru, 1978; Tsang et al., 1985):

$$Z_{aFS}(\Omega_o,r) \equiv Z_e(r) L^2(r) \quad (12b)$$

It is worth mentioning that, by inserting (12b) in (10), we re-obtain the classical radar equation given by (1). Equation (12) holds only if single-scattering hypotheses can be assumed for the considered frequency in a moderately attenuating medium.

In order to numerically evaluate the influence of incoherent backscattering on the measured radar reflectivity, the radar received power due to multiple scattering must be computed as a function of the distance r. Using formulas (7) and (12a) implies the computation of $<I_R(\Omega_o,r)>_{MS}$ and $<I_R(\Omega_o,r)>_{FS}$, respectively. A previously developed three-dimensional (3-D) Monte Carlo method, making use of a biasing technique in order to reduce the computational time, was adapted to the considered radar observation geometry by adopting a forward scheme (Roberti, 1997). The choice of a Monte Carlo solution was also suggested by the strict analogy between the algorithm flow chart and the radar observation mechanism.

A plane-parallel geometry was considered characterizing each layer by means of the hydrometeor contents and optical parameters, shown in Figs. 1 and 2. Even if the adopted Monte Carlo method has 3-D capabilities, a 1-D framework was adopted in order to better focus on the multiple scattering effects, thus avoiding unnecessary complications. A Lambertian surface with a constant reflectivity of 0.1 was considered for modeling the surface. Notice that the case of a low surface reflectivity (e.g., ground surface) allows us to single out the atmospheric scattering effects. A collimated radar beam with power density $F_T(\Omega_o,r)$ was supposed to be incident upon the top boundary of the cloud profiles in the nadir direction. It is worth mentioning that backscattering enhancement was not considered in this work since it should be negligible in the interaction between microwaves and hydrometeors (Ito et al., 1995). Both $Z_{aMS}(\Omega_o,r)$ and $Z_{aFS}(\Omega_o,r)$ were computed at nadir from (7) and (12), respectively.

4. Numerical results

As already sketched in sect. 2, the numerical simulation was carried out for spaceborne radar observations at nadir with a range resolution of 500 m (corresponding to a pulse duration Δt of 3.3 μs) for the three frequency bands at 13.8, 24, and 35 GHz. The receiver was assumed to be able to process contiguous range bins. The minimum detectable reflectivity factor was taken to be 10 dBZ for numerical purposes, even though realistic minimum values should go approximately from 5 dBZ at 13.8 GHz to 0 dBZ at 35 GHz (Testud et al., 1992; Kummerow et al., 1998).

As demonstrated in the previous section, the *apparent* radar reflectivity can be evaluated from the received specific mean intensity. Figs. 3 and 4 show both the *apparent* reflectivity factor Z_{aMS}, given by (9) and taking into account multiple scattering effects, and the reflectivity factor Z_{aFS}, given by (12) and taking into account only

single scattering effects, at 14 and 35 GHz for the LRF and IRF cases, as a function of the altitude (distance at nadir).

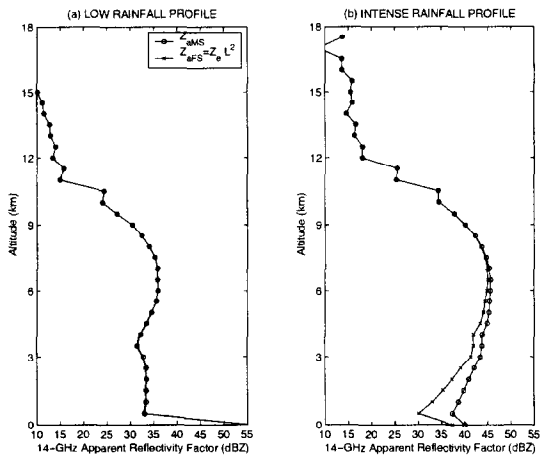

Fig. 3. Nadir profiles of *apparent* reflectivity factor Z_{aMS}, given by (9) and taking into account multiple scattering effects, and of Z_{aFS}, given by (12) and taking into account only first-order scattering effects, at 14 GHz for the LRF and IRF cases as a function of the altitude.

At 14 GHz and for LRF, all the reflectivities tend to coincide as reasonable since the atmospheric albedo and attenuation are negligible. At low frequency and for low to moderate rainfall, the surface scattering is predominant. The surface influence is quickly masked by rain and graupel scattering as the frequency and rainfall increase; correspondingly, the first-order scattering approximation becomes inadequate for altitudes below the freezing level. As the frequency increases, the altitude of the initial departure between Z_e and Z_{aMS} becomes higher and higher going from 5 km at 14 GHz (freezing level) to about 9 km (top height of graupel layers) at 35 GHz. This is also explained by looking at the behavior of path attenuation, that is the difference between Z_{aFS} and Z_e.

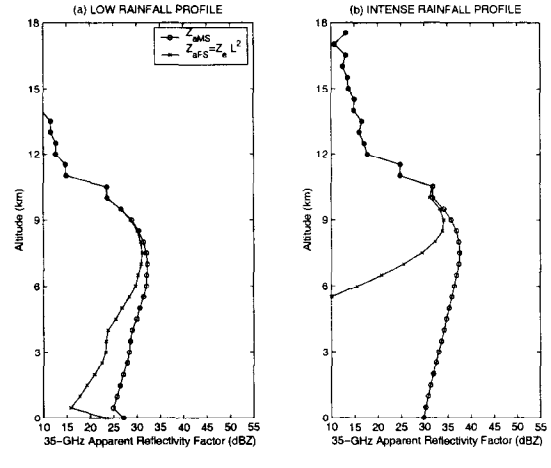

Fig. 4. Same as in Fig. 3, but at 35 GHz.

The difference between Z_{aMS} e Z_{aFS} gives a quantitative indication of the multiple scattering effects, while the difference between Z_{aFS} e Z_e provides a measure of the path attenuation effects as deductible from (12b). As expected, it holds for all the cases $Z_{aFS}<Z_{aMS}<Z_e$. Simulated Z_{aMS} compares favorably with measurements at 14 and 35 GHz (e.g.,, Kumagai et al., 1993), even though the 35-GHz Z_{aMS} close to the surface appears to be higher than measured ones due to the surface scattering model choice.

The previous figures prove that opposite effects are due to the combination of path attenuation and multiple scattering. On one hand, path attenuation is predominant for the single-scattering case and tends to reduce the equivalent reflectivity, especially at longer distances from the radar. On the other hand, multiple scattering tends to increase the single-scattering reflectivity, especially in the cloud regions characterized by large albedo, even though the effect of path attenuation still reduces its values with respect to the equivalent reflectivity ones.

As usually done in the radar inverse problem, the profile of the rainrate R can be derived from a power relationship using the estimated equivalent reflectivity Z. Various Z-R have been proposed in literature, mainly depending on the storm type and working frequency (Sauvageot, 1992). As an example, we have chosen a relation derived from the analysis of airborne microphysical data during an experimental campaign observing a tropical squall-line precipitation event. By assuming a Marshall-Palmer (MP) drop size distribution, the Z-R formula valid at 13.8 GHz is (Marecal et al., 1997):

$$Z = 265.5\, R^{1.614} \tag{13}$$

where Z is in mm^6m^{-3} and R in mm/h. Note that the precipitation type and the constant intercept N_o=8.0 10^6 m^{-4} of the MP drop-size distribution, assumed to derive (13), are consistent with the modeling ones.

Fig. 5 gives an example of the retrieved rainrate profile, derived from (13), for the LRF and IRF cases as a function of the altitude. For computing R we used the equivalent reflectivity factor Z_e, that is $Z=Z_e$ in (13), and the *apparent* reflectivity factors Z_{aMS} taking into account the path attenuation factor L, that is using in (13) $Z=Z_{aMS}/L^2$. Only R values at altitudes greater than 1 km are shown in order to avoid the surface contamination. Notice that (13) is strictly valid only for rain layers, that is below the freezing level.

As expected, for low rainfall the multiple scattering effects are negligible and the rainrate profiles, recomputed from $Z=Z_{aFS}/L^2=Z_e$ and from $Z=Z_{aMS}/L^2$, are practically coincident. For intense rainfall, the use of $Z=Z_{aMS}/L^2$ shows that path attenuation correction does not provide a reconstruction of the "true" R profile, derived from Z_e, thus indicating the non-adequateness of first-order scattering assumption at 14 GHz for IRF. Looking at the discrepancies in terms of rainrate R, the difference between the "true" value and that one derived from Z_{aMS}/L^2 are almost zero for LRF. For IRF the 'true' R can be up to 50% lower than the one derived from Z_{aMS}/L^2.

Previous results suggest that, when multiple scattering is relevant, the correction of Z_{aMS} by means of the path attenuation factor L^2 gives rise to an overestimation of the

equivalent reflectivity. This means that *apparent* path attenuation (smaller than "true" single-scattering attenuation A), taking into account multiple scattering effects, should be evaluated for properly correcting *apparent* (measured) reflectivity. This might be accomplished, for instance, by an adaptive surface reference technique (Iguchi and Meneghini, 1994).

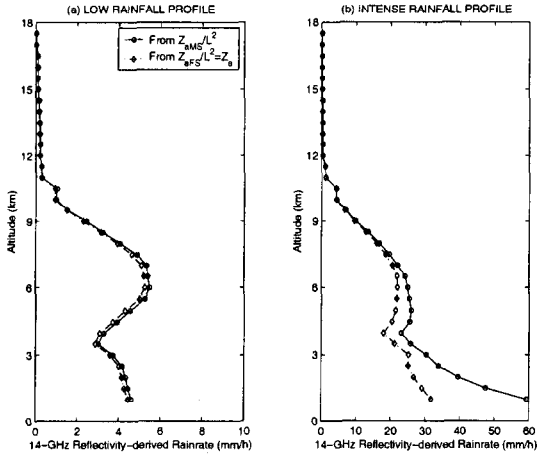

Fig. 5. Nadir profiles of retrieved rainrate derived from the Z-R relation at 14 GHz, given by (13), using for Z: i) the equivalent reflectivity factor, i.e. $Z=Z_{aFS}/L^2=Z_e$; ii) the multiple-scattering *apparent* reflectivity factor taking into account the two-way path-integrated attenuation, i.e. $Z=Z_{aMS}/L^2$.

5. Summary and conclusions

Spaceborne radar observations of precipitation profiles were simulated by means of a radiative transfer model, using a Monte Carlo solution technique. The effects of precipitation multiple scattering were evaluated at various attenuating frequencies and for nadir observations. The PR 13.8-GHz frequency band was chosen together with the envisaged channels at 24 GHz and 35 GHz.

Realistic precipitation profiles were extracted from a microphysical mesoscale cloud model, simulating an intense squall line. In order to better interpret the results, the hydrometeor vertical profiles were grouped in 2 categories going from low to intense rainfall. Equivalent reflectivity, volumetric albedo and path attenuation were computed and discussed, noting the relevant impact of graupel particles at frequencies above Ku band.

Numerical results showed that the difference between multiple-scattering reflectivity factor (Z_{aMS}) and the single-scattering one (Z_{aFS}) can give an indication of the multiple scattering effects, while the difference between Z_{aFS} and the equivalent reflectivity factor Z_e provides a measure of the path attenuation effects. As expected, it holds for all the cases $Z_{aFS}<Z_{aMS}<Z_e$. When converting reflectivity in rainrate profiles through a Z-R relation at 14 GHz for intense rainfall, the "true" R value can be up to about 50% lower that one derived from Z_{aMS}/L^2. *Apparent* path attenuation should be properly evaluated in multiple scattering conditions to reconstruct equivalent reflectivity from *apparent* reflectivity measurements.

Acknowledgements. This work was partially supported by the Italian Space Agency (ASI) and by the European Union through the Euro-TRMM project. The authors would like to thank Dr. Kummerow from NASA/GSFC (Greenbelt, MD) for making the cloud model available.

References

Fujita, M., "An algorithm for estimating rain rate by a dual-frequency radar", *Radio Sci*, 18, 697-708, 1983.

Kummerow, C., W. Barnes, T. Kozu, J. Shiue, and J. Simpson, "The Tropical Rainfall Measuring Mission (TRMM) sensor package", *J. Atmos. Ocean. Tech.*, 15, 809-817, 1998.

Haddad, Z., E. Im, and S.L. Durden, "Optimal estimation of rain-rate profiles from single-frequency radar echoes", *J. Appl. Meteor.*, 35, 214-228, 1996.

Iguchi, T., and R. Meneghini, "Intercomparison of single-frequency methods for retrieving a vertical rain profile from an airborne or spaceborne radar data," *J. Atmos. Oceanic Tech.*, 11, 1507-1516, 1994.

Ishimaru, A., *Wave propagation and scattering in random media*, vol. 1 and 2, Academic Press, New York, 1978.

Ito, S., T. Oguchi, T. Iguchi, H. Kumagai, and R. Meneghini, "Depolarization of radar signals due to multiple scattering in rain", *IEEE Trans. Geosci. Remote Sens.*, 33, 1057-1062, 1995.

Kumagai, H., R. Meneghini, and T. Kozu, "Preliminary results from multiparameter airborne rain radar measurement in the Western Pacific", *J. Appl. Meteor.*, 36, 431-440, 1993.

Marecal, V., T. Tani, P. Amayenc, C. Klapisz, E. Obligis, and N. Viltard, "Rain relations inferred from microphysical data in TOGA-COARE and their use to test a rain-profiling method from radar measurements at Ku-band", *J. Appl. Meteor.*, 36, 1629-1646, 1997.

Marzano, F.S., A. Mugnai, E.A. Smith, X. Xiang, J. Turk, and J. Vivekanandan, "Active and passive remote sensing of precipitating storms during CaPE. Part II: Intercomparison of precipitation retrievals from AMPR radiometer and CP-2 radar", *Meteor. Atmospheric Physics*, 54, 29-51, 1994.

Marzano, F.S., A. Mugnai, G. Panegrossi, N. Pierdicca, E.A. Smith, and J. Turk, "Bayesian estimation of precipitating cloud parameters from combined measurements of spaceborne microwave radiometer and radar", *IEEE Trans. Geosci. Rem. Sens.*, 37, 596-613, 1999.

Marzoug, M., and P. Amayenc, "A class of single and dual frequency algorithms for rain-rate profiling from a spaceborne radar. Part I: Principle and tests from numerical simulations", *J. Atmos. Oceanic Technol.*, 11, 1480-1506, 1994.

Meneghini, R., "Rain rates estimates for an attenuating radar", *Radio Sci.*,13 , 459-470, 1978.

Meneghini, R., and K. Nakamura, "Range profiling of the rain rate by an airborne weather radar", *Remote Sens. Environ.*, 31, 193-209, 1990.

Mongi, M., and P. Amayenc, "Improved range-profiling algorithm of rainfall rate from a spaceborne radar with path-integrated attenuation constraint", *IEEE Trans. Geosci. Remote Sens.*, 29, 584-592, 1991.

Oguchi, T., N. Ishida, and T. Ihara, "Effect of multiple scattering on the estimation of rainfall rates using a dual wavelenght radar techniques", *IEEE Trans. Geosci. Rem. Sensing*, 32, 943-946, 1994.

Olson, W.S., C.D. Kummerow, G.M. Heymsfield, and L. Giglio, "A method for combined passive-active microwave retrievals of cloud and precipitation parameters," *J. Appl. Meteor.*, 35, 1763-1789, 1996.

Roberti, L., "Monte Carlo radiative transfer in the microwave and in the visible: biasing techniques", *Appl. Opt.*, 36, 7929-7938, 1997.

Sauvageot, H., *Radar meteorology*, Artech House, Norwood (MA), 1992.

Tao, K., J. Simpson, and S.T. Soong, "Statistical properties of a cloud ensemble: a numerical study", *J. Atm. Sci.*, 44, 3175-3187, 1987.

Testud, J., P. Amayenc, and M. Marzoug, "Rainfall-rate retrieval from a spaceborne radar: comparison between single-frequency, dual-frequency and dual-beam techniques," *J. Atmos. Ocean. Techn.*, 9, 599-623, 1992.

Tsang, L., J.A. Kong, and R.T. Shin, *Theory of microwave remote sensing*, J. Wiley & Sons, New York (NY), 1985.